Science Advances
AAAS

Supplementary Materials for

Direct growth of wafer-scale highly-oriented graphene on sapphire

Zhaolong Chen, Chunyu Xie, Wendong Wang, Jinpei Zhao, Bingyao Liu, Jingyuan Shan, Xueyan Wang, Min Hong, Li Lin, Li Huang, Xiao Lin, Shenyuan Yang*, Xuan Gao, Yanfeng Zhang*, Peng Gao*, Kostya S. Novoselov*, Jingyu Sun*, Zhongfan Liu*

*Corresponding author. Email: syyang@semi.ac.cn (S.Y.); yanfengzhang@pku.edu.cn (Y.Z.); p-gao@pku.edu.cn (P.G.); kostya@nus.edu.sg (K.S.N.); sunjy86@suda.edu.cn (J.S.); zfliu@pku.edu.cn (Z.L.)

Published 19 November 2021, *Sci. Adv.* **7**, eabk0115 (2021)
DOI: 10.1126/sciadv.abk0115

This PDF file includes:

Supplementary Text

DFT computational details.

The first-principles calculations based on DFT are carried out using the Vienna *Ab-initio* simulation package (VASP) (*44*). We adopt the all-electron-like projector-augmented wave potentials (45) and the generalized-gradient approximation of Perdew, Burke, and Ernzerhof (PBE) (46) for the exchange correlation functional. The energy cutoff for the plane-wave expansion is set as 400 eV. The surface of Al-terminated Al_2O_3(0001) is constructed with (1×1) periodicity and an expanded (3×3) supercell is chosen to support the modelling of graphene cluster adsorption. The graphene cluster $C_{24}H_{12}$ is adsorbed on such a supercell at different adsorption sites and different rotational angles. The Al-terminated Al_2O_3(0001) surface is modeled by an eight-layer slab with the bottom passivated by pseudo-hydrogen atoms. These pseudo-hydrogen atoms and the three bottom layers of Al_2O_3 slab are kept fixed during the relaxation. The coordinates of atoms are relaxed until the Hellmann-Feynman forces on each atom are less than 0.01 eV/Å. The thickness of the vacuum region is about 18 Å, which is large enough to reduce the interaction between images. A 2×2×1 Monkhorst-Pack k-point mesh is used for the Brillouin zone sampling (47). Weak van der Waals (vdW) interactions are included with the Becke88 optimization (optB88) functional (48).

Adsorption sites for $C_{24}H_{12}$ cluster on Al_2O_3 substrate.

We test different adsorption sites for graphene cluster $C_{24}H_{12}$ on Al_2O_3 substrate: with one C atom on top of the surface low-Al atom (**Fig. 1d**), and with the center of the cluster (also the center of the six-member ring) on top of the low-Al atom (**fig. S2a**). Our calculations show that the latter is less stable than the the former. As shown in **fig. S2b**, when the center is positioned on top of the surface low-Al atom, the total enegy is always higher than those with C atom on top of low-Al atom at all the considered rotational angles (θ = 0°~30°). Besides, the lowest energy for this configuration corresponds to rotational angle of 0° rather than 30°, inconsistent with the experiment observations. Therefore, we only consider the configurations with C atom on top of surface low-Al atom when we determine the preferred rotational angle.

Adsorption geometry of $C_{24}H_{12}$ cluster on Al_2O_3 substrate without constraint.

To maintain the rotational angle, the in-plane coordinates of two C atoms are kept fixed during relaxation. The constraint would also overestimate the energy of the adsorption structures. To obtain the more reliable energies at local minima, we remove the constraint and fully relax the adsorption structures at rotational angles of 0°, 30° and 60° (hollow symbols in **fig. S2b**). As shown in **fig. S3**, the $C_{24}H_{12}$ cluster will slightly shift on the substrate, such that more C atoms get closer to the surface low-Al atoms. At the rotational angle of 30°, there are four such C atoms that are almost on top of the surface low-Al atoms (denoted by arrows in **fig. S3b**). Therefore, this configuration has a lower energy than those with rotational angles of 0° and 60° by about 0.2 eV. We note that the adsorption of $C_{24}H_{12}$ cluster on sapphire substrate is dominant by van der Waals interaction. The adsorption energy per atom is around 0.07~0.08 eV, similar to that of graphene layer on the same substrate. Despite of its weak nature, the registry of van der Waals interaction is strong enough to lead to the energy-minimal configuration at rotational angle of 30°.

Fig. S1. Photograph of homemade induction heating CVD system. Insect is the schematic illustration of the growth of graphene on sapphire wafer.

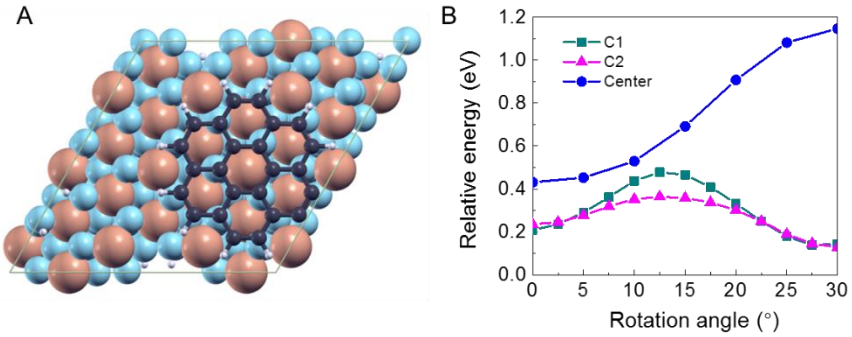

Fig. S2. First-principles calculations of the relative energies of graphene cluster $C_{24}H_{12}$ on an Al_2O_3 (0001) substrate. (A) The atomic structure of graphene cluster $C_{24}H_{12}$ on Al_2O_3 (0001) surface with the center on top of the surface low-Al atom at rotational angle of 30°. (B) Relative energies as a function of rotational angles of the adsorption structure shown in (A). The relative energies with C1 and C2 atoms on top of low-Al atom are also shown for comparison.

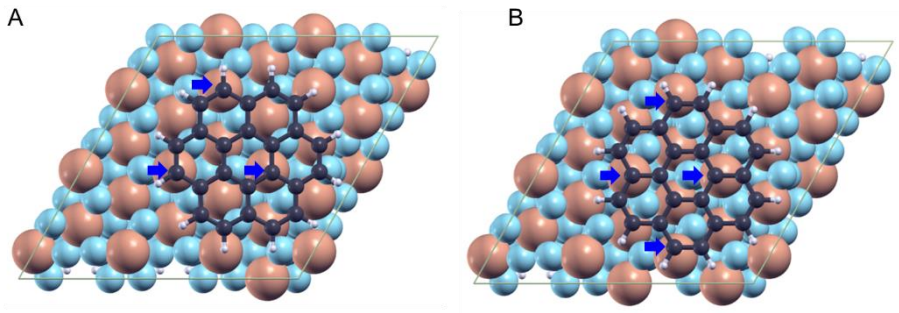

Fig. S3. The relaxed geometries of graphene cluster $C_{24}H_{12}$ on Al_2O_3 (0001) surface without constraint. The atomic structure of graphene cluster $C_{24}H_{12}$ on Al_2O_3 (0001) surface at rotational angles of 0^o (A) and 30^o (B). The arrows denote the C atoms that are almost on top of the surface low-Al atoms.

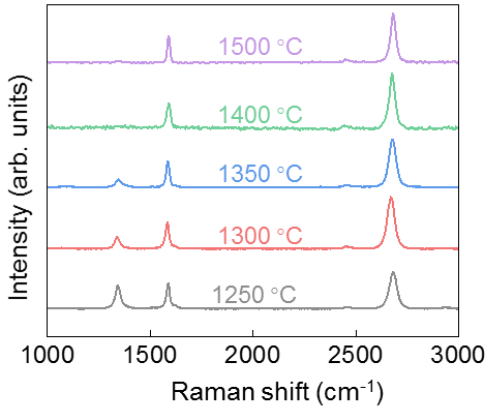

Fig. S4. Raman spectra of the temperature-dependent growth of graphene on sapphire. All the spectra have been normalized to G-band intensity of each spectrum. The D-band intensity decreases with elevating temperature, indicative of the reduced defect densities in graphene.

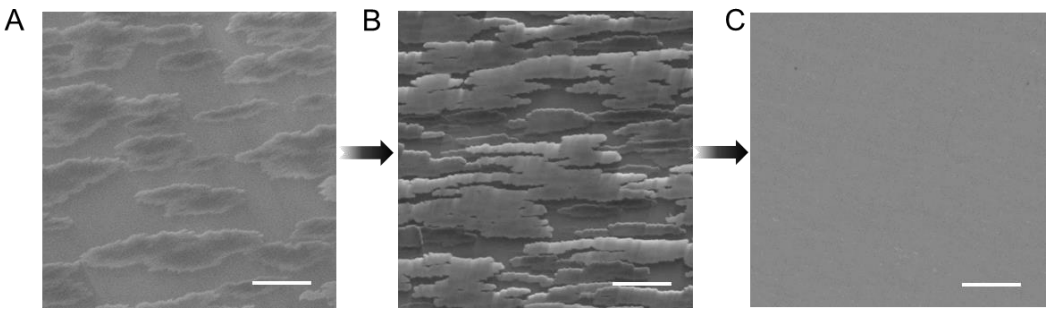

Fig. S5. SEM images of as-grown graphene on the Al_2O_3 (0001) substrate measured at representative positions with increased growth time. The evolutions from individual domains

to continues film with increased growth time of 10 min (A), 15 min (B), and 30 min (C), respectively, (1400 °C, 2000 Pa, Ar/H_2/CH_4: 1000/500/1100 sccm). Scale bars: 20 μm. The formation of such quasi-rectangle shaped graphene domains is a consequence of the high energy barriers of a graphene bridging the Al_2O_3 steps (**fig. S13**) in the forward direction and relatively fast propagation on the plateau in between neighbouring step.

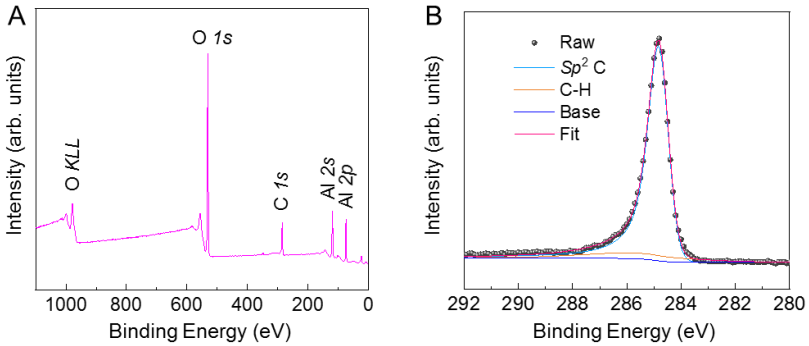

Fig. S6. XPS spectra of the directly grown graphene/sapphire sample. (A) Full-range XPS spectrum of the directly grown graphene on sapphire. (B) C *1s* XPS spectrum shows the characteristic signals of graphene with a predominant sp^2 carbon peak (~284.8 eV) and a weak C–H peak (285.5 eV). Because the C *1s* peak of graphene is usually asymmetric (*49*), we used an asymmetric line shape for fitting the spectrum (*50*).

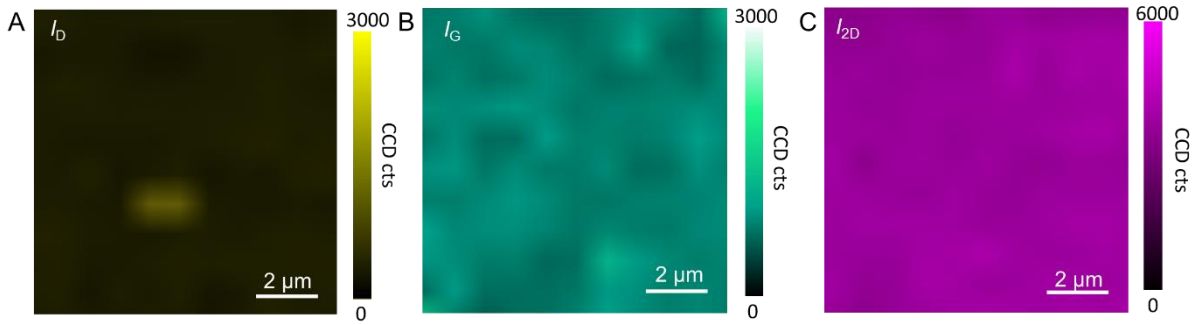

Fig. S7. Raman D, G and 2D band intensity map of as-grown graphene films on sapphire by electromagnetic induction heating cold-wall CVD.

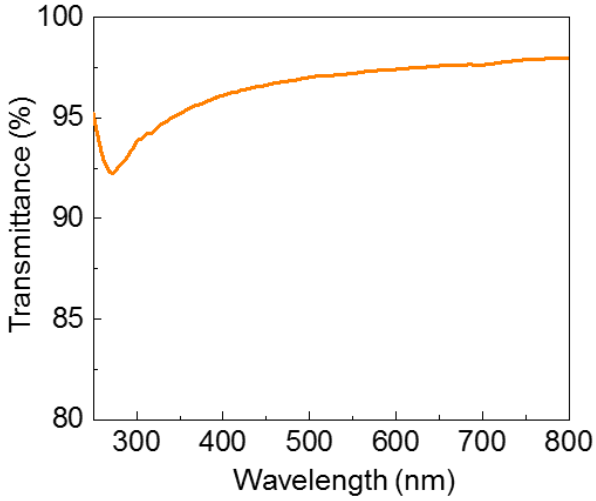

Fig. S8. Typical UV–vis spectrum of as-grown graphene film.

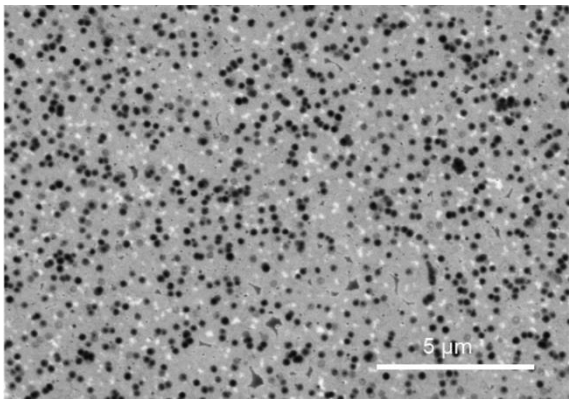

Fig. S9. Typical SEM image of the conventional hot-wall CVD derived graphene film on sapphire (3-inch sized quartz tube chamber; 1100 °C; Ar/H_2/CH_4: 500/50/12 sccm; 120 min). The black spots are the amorphous carbon/multilayer region originating from the rampant gas-phase side-reactions.

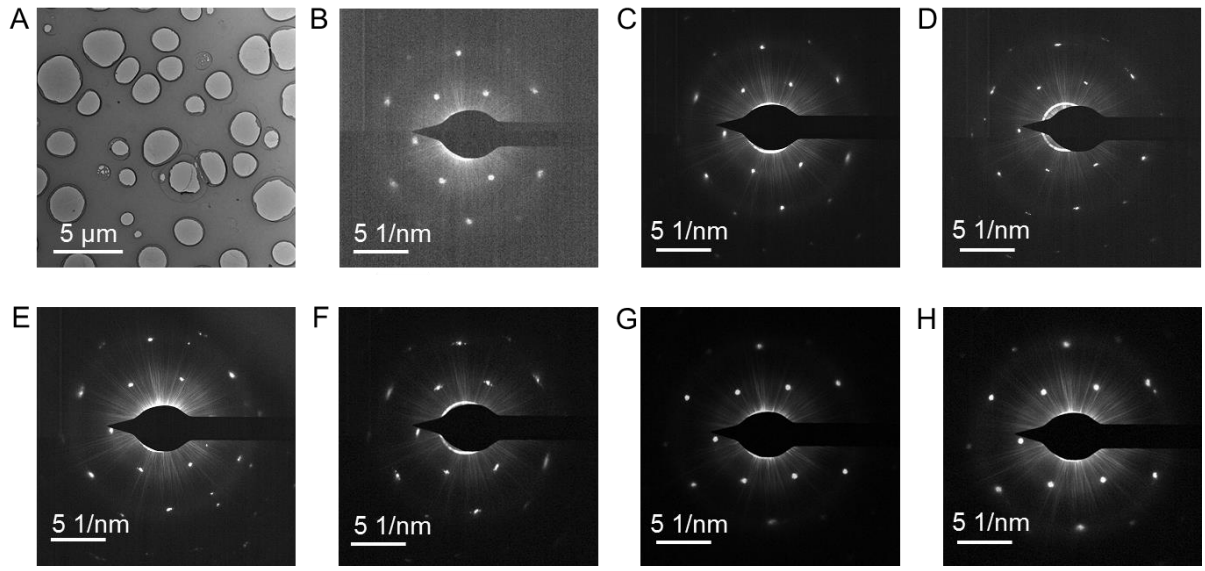

Fig. S10. SAED patterns of graphene. (A) TEM image of the as-grown graphene film after transferring onto a copper grid. (B-H) The remaining images are the SAED patterns of graphene collected in such an area.

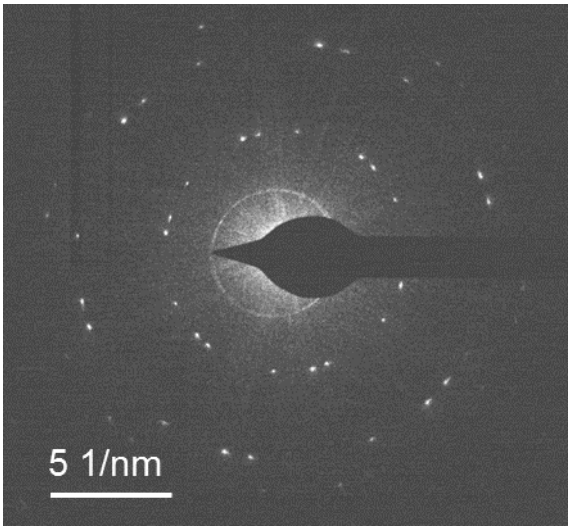

Fig. S11. Typical SAED pattern of conventional hot-wall CVD derived graphene film on sapphire (3-inch sized quartz tube chamber; 1100 °C; $Ar/H_2/CH_4$: 500/50/12 sccm; 120 min). It can be observed that multiple sets of diffraction points are presented, indicating that low temperature growth usually leads to a polycrystalline film consisted of randomly orientated small domains.

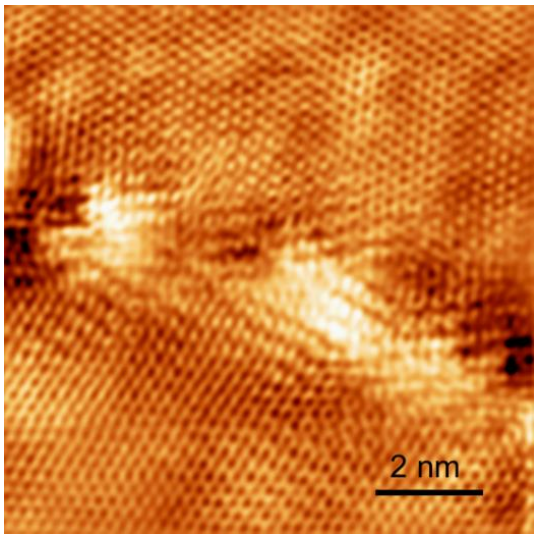

Fig. S12. An atomically resolved STM image of the domain boundary of as-grown graphene on sapphire, showing the seamless stitching growth mode.

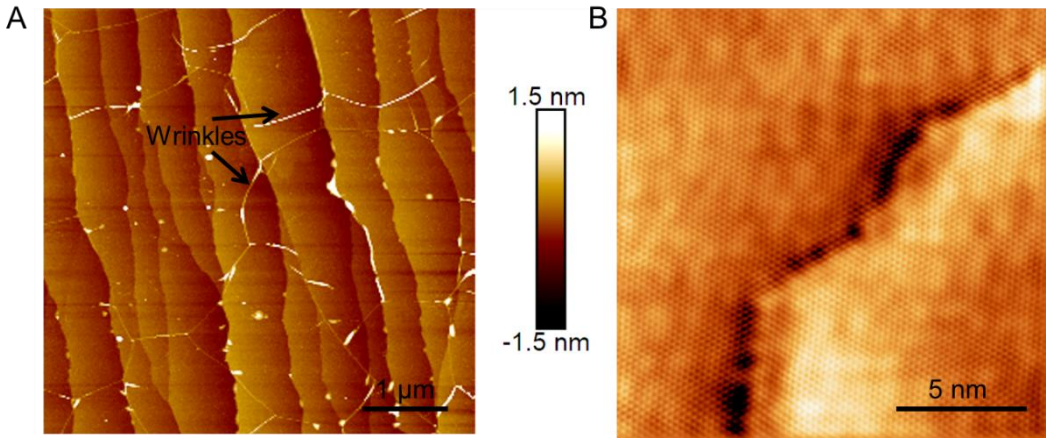

Fig. S13. SPM images of the graphene directly grown on Al_2O_3. (A) AFM height image of the graphene/sapphire substrate upon CVD reaction, demonstrating the formation of atomic terraces of Al_2O_3 after graphene growth. (B) STM image of the graphene crossing over the step of Al_2O_3.

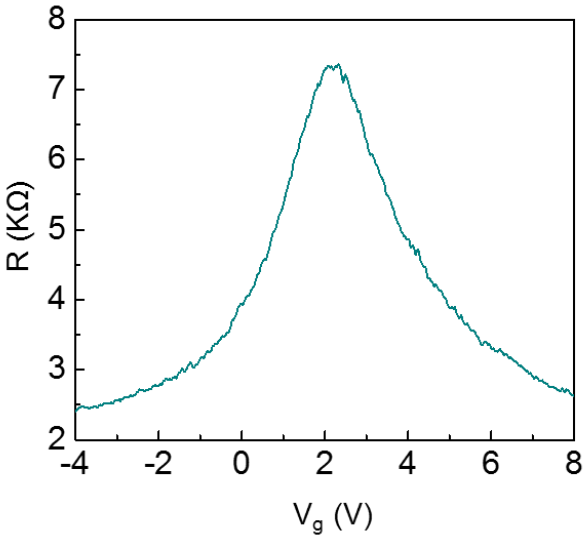

Fig. S14. Resistance of graphene *vs.* top-gate voltage curve. The nonlinear fitting of mobility is ~9500 cm^2 V^{-1} s^{-1} (T = 300 K).

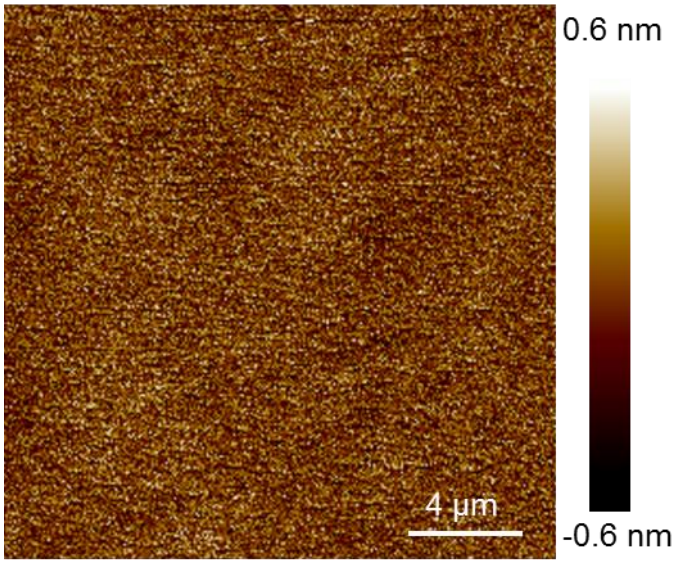

Fig. S15. AFM height image of a sapphire surface after annealing in a H_2/Ar atmosphere at 1400 °C for about 5 min, showing a clean and atomically flat surface.

Table S1. Comparison of the carrier mobility values between our directly gown graphene on sapphire in this work and previously reported graphene grown on typical dielectric and catalytic substrates.

	This work	Sapphire	SiO_2	BN	Cu	Ni
Carrier Mobility ($cm^2 V^{-1} s^{-1}$) & (Carrier Density (cm^{-2})) at 300 K	9500 (9.0×10^{11})	3000 (4.5×10^{11}) (*30*); 370 (none) (32); 2000 (3×10^{11}) (33)	531 (none) (*18*); 900 (none) (*23*); 3800 (none) (*25*)	17000 (none) (*51*)	4365 (0.9 to 2.6×10^{12}) (*52*); 11000 (none) (*53*)	3700 (9.0×10^{12}) (*16*)

Table S2. Comparison of methodology features between our developed growth strategy and previously reported epitaxial growth on SiC, demonstrating the advantages of our strategy in terms of low cost and high efficiency in obtaining high-quality graphene films.

	Cost of substrate	Growth Conditions	I_D/I_G	Mobility ($cm^2 V^{-1} s^{-1}$) & (Carrier Density (cm^{-2})) at 300 K	Uniformity (coverage of monolayer)	Potential Applications
This Work	~10 $ (2 in.); ~20 $ (4 in.)	1400 °C, 0.5 h, 2000 Pa	<0.05	9500 (9.0×10^{11})	>95 %	high frequency transistors; transparent electrodes; LED; microelectronics
Epitaxy on SiC	~300 $ (2 in.); ~650 $ (4 in.)	>1500 °C, 0.2-1 h, Ar atmosphere (*9,38*); High vacuum (0.1-10^{-4} Pa) (8)	0.05-0.15 (*9, 54, 55*)	5,800 (~2 × 10^{12}) on Si face (8); 150,000 (~1.5 × 10^{12}) on C face (8); 1,660 (1.79 × 10^{12}) on Si face (9); 2800 (8.1 × 10^{11}) on Si face (*11*); 900 (1 × 10^{13}) on Si face (*38*); 2,500 (none) after transferring on SiO_2 (*55*)	~85% (*38*)	transistors; customer electronics

REFERENCES AND NOTES

1. K. S. Novoselov, V. I. Fal'ko, L. Colombo, P. R. Gellert, M. G. Schwab, K. Kim, A roadmap for graphene. *Nature* **490**, 192–200 (2012).

2. Y. Wu, Y.-m. Lin, A. A. Bol, K. A. Jenkins, F. Xia, D. B. Farmer, Y. Zhu, P. Avouris, High-frequency, scaled graphene transistors on diamond-like carbon. *Nature* **472**, 74–78 (2011).

3. S. Bae, H. Kim, Y. Lee, X. Xu, J.-S. Park, Y. Zheng, J. Balakrishnan, T. Lei, H. R. Kim, Y. I. Song, Y.-J. Kim, K. S. Kim, B. Ozyilmaz, J.-H. Ahn, B. H. Hong, S. Iijima, Roll-to-roll production of 30-inch graphene films for transparent electrodes. *Nat. Nanotechnol.* **5**, 574–578 (2010).

4. F. Xia, T. Mueller, Y.-m. Lin, A. Valdes-Garcia, P. Avouris, Ultrafast graphene photodetector. *Nat. Nanotechnol.* **4**, 839–843 (2009).

5. M. Liu, X. Yin, E. Ulin-Avila, B. Geng, T. Zentgraf, L. Ju, F. Wang, X. Zhang, A graphene-based broadband optical modulator. *Nature* **474**, 64–67 (2011).

6. T. Wu, X. Zhang, Q. Yuan, J. Xue, G. Lu, Z. Liu, H. Wang, H. Wang, F. Ding, Q. Yu, X. Xie, M. Jiang, Fast growth of inch-sized single-crystalline graphene from a controlled single nucleus on Cu-Ni alloys. *Nat. Mater.* **15**, 43–47 (2016).

7. J.-H. Lee, E. K. Lee, W.-J. Joo, Y. Jang, B.-S. Kim, J. Y. Lim, S.-H. Choi, S. J. Ahn, J. R. Ahn, M.-H. Park, C.-W. Yang, B. L. Choi, S.-W. Hwang, D. Whang, Wafer-scale growth of single-crystal monolayer graphene on reusable hydrogen-terminated germanium. *Science* **344**, 286–289 (2014).

8. J. L. Tedesco, B. L. VanMil, R. L. Myers-Ward, J. M. McCrate, S. A. Kitt, P. M. Campbell, G. G. Jernigan, J. C. Culbertson, C. R. Eddy Jr., D. K. Gaskill, Hall effect mobility of epitaxial graphene grown on silicon carbide. *Appl. Phys. Lett.* **95**, 122102 (2009).

9. E. Pallecchi, F. Lafont, V. Cavaliere, F. Schopfer, D. Mailly, W. Poirier, A. Ouerghi, High electron mobility in epitaxial graphene on 4H-SiC (0001) via post-growth annealing under hydrogen. *Sci. Rep.* **4**, 4558 (2014).

10. Y.-M. Lin, A. Valdes-Garcia, S.-J. Han, D. B. Farmer, I. Meric, Y. Sun, Y. Wu, C. Dimitrakopoulos, A. Grill, P. Avouris, K. A. Jenkins, Wafer-scale graphene integrated circuit. *Science* **332**, 1294–1297 (2011).

11. M. Kruskopf, D. M. Pakdehi, K. Pierz, S. Wundrack, R. Stosch, T. Dziomba, M. Götz, J. Baringhaus, J. Aprojanz, C. Tegenkamp, Comeback of epitaxial graphene for electronics: Large-area growth of bilayer-free graphene on SiC. *2D Mater.* **3**, 041002 (2016).

12. P. R. Whelan, V. Panchal, D. H. Petersen, D. M. Mackenzie, C. Melios, I. Pasternak, J. Gallop, F. W. Østerberg, P. U. Jepsen, W. Strupinski, O. Kazakova, P. Bøggild, Electrical homogeneity mapping of epitaxial graphene on silicon carbide. *ACS Appl. Mater. Interfaces* **10**, 31641–31647 (2018).

13. N. Mishra, S. Forti, F. Fabbri, L. Martini, C. McAleese, B. R. Conran, P. R. Whelan, A. Shivayogimath, B. S. Jessen, L. Buß, J. Falta, I. Aliaj, S. Roddaro, J. I. Flege, P. Bøggild, K. B. K.

Teo, C. Coletti, Wafer-scale synthesis of graphene on sapphire: Toward fab-compatible graphene. *Small* **15**, 1904906 (2019).

14. X. Xu, Z. Zhang, L. Qiu, J. Zhuang, L. Zhang, H. Wang, C. Liao, H. Song, R. Qiao, P. Gao, Z. Hu, L. Liao, Z. Liao, D. Yu, E. Wang, F. Ding, H. Peng, K. Liu, Ultrafast growth of single-crystal graphene assisted by a continuous oxygen supply. *Nat. Nanotechnol.* **11**, 930–935 (2016).

15. Y. Hao, M. S. Bharathi, L. Wang, Y. Liu, H. Chen, S. Nie, X. Wang, H. Chou, C. Tan, B. Fallahazad, H. Ramanarayan, C. W. Magnuson, E. Tutuc, B. I. Yakobson, K. F. McCarty, Y.-W. Zhang, P. Kim, J. Hone, L. Colombo, R. S. Ruoff, The role of surface oxygen in the growth of large single-crystal graphene on copper. *Science* **342**, 720–723 (2013).

16. K. S. Kim, Y. Zhao, H. Jang, S. Y. Lee, J. M. Kim, K. S. Kim, J.-H. Ahn, P. Kim, J.-Y. Choi, B. H. Hong, Large-scale pattern growth of graphene films for stretchable transparent electrodes. *Nature* **457**, 706–710 (2009).

17. Z. Zhang, J. Du, D. Zhang, H. Sun, L. Yin, L. Ma, J. Chen, D. Ma, H.-M. Cheng, W. Ren, Rosin-enabled ultraclean and damage-free transfer of graphene for large-area flexible organic light-emitting diodes. *Nat. Commun.* **8**, 14560 (2017).

18. J. Chen, Y. Wen, Y. Guo, B. Wu, L. Huang, Y. Xue, D. Geng, D. Wang, G. Yu, Y. Liu, Oxygen-aided synthesis of polycrystalline graphene on silicon dioxide substrates. *J. Am. Chem. Soc.* **133**, 17548–17551 (2011).

19. W. Yang, G. Chen, Z. Shi, C.-C. Liu, L. Zhang, G. Xie, M. Cheng, D. Wang, R. Yang, D. Shi, K. Watanabe, T. Taniguchi, Y. Yao, Y. Zhang, G. Zhang, Epitaxial growth of single-domain graphene on hexagonal boron nitride. *Nat. Mater.* **12**, 792–797 (2013).

20. M. Kolmer, R. Zuzak, A.-K. Steiner, L. Zajac, M. Engelund, S. Godlewski, M. Szymonski, K. Amsharov, Fluorine-programmed nanozipping to tailored nanographenes on rutile TiO_2 surfaces. *Science* **363**, 57–60 (2019).

21. M. Kolmer, A.-K. Steiner, I. Izydorczyk, W. Ko, M. Engelund, M. Szymonski, A.-P. Li, K. Amsharov, Rational synthesis of atomically precise graphene nanoribbons directly on metal oxide surfaces. *Science* **369**, 571–575 (2020).

22. Z. Chen, Y. Qi, X. Chen, Y. Zhang, Z. Liu, Direct CVD growth of graphene on traditional glass: Methods and mechanisms. *Adv. Mater.* **31**, 1803639 (2019).

23. H. Kim, I. Song, C. Park, M. Son, M. Hong, Y. Kim, J. S. Kim, H.-J. Shin, J. Baik, H. C. Choi, Copper-vapor-assisted chemical vapor deposition for high-quality and metal-free single-layer graphene on amorphous SiO_2 substrate. *ACS Nano* **7**, 6575–6582 (2013).

24. P.-Y. Teng, C.-C. Lu, K. Akiyama-Hasegawa, Y.-C. Lin, C.-H. Yeh, K. Suenaga, P.-W. Chiu, Remote catalyzation for direct formation of graphene layers on oxides. *Nano Lett.* **12**, 1379–1384 (2012).

25. H. Wang, X. Xue, Q. Jiang, Y. Wang, D. Geng, L. Cai, L. Wang, Z. Xu, G. Yu, Primary nucleation-dominated chemical vapor deposition growth for uniform graphene monolayers on dielectric substrate. *J. Am. Chem. Soc.* **141**, 11004–11008 (2019).

26. L. Cui, X. Chen, B. Liu, K. Chen, Z. Chen, Y. Qi, H. Xie, F. Zhou, M. H. Rummeli, Y. Zhang, Z. Liu, Highly conductive nitrogen-doped graphene grown on glass toward electrochromic applications. *ACS Appl. Mater. Interfaces* **10**, 32622–32630 (2018).

27. T. Baehr-Jones, A. Spott, R. Ilic, A. Spott, B. Penkov, W. Asher, M. Hochberg, Silicon-on-sapphire integrated waveguides for the mid-infrared. *Opt. Express* **18**, 12127–12135 (2010).

28. Z. Chen, P. Gao, Z. Liu, Graphene-based LED: From principle to devices. *Acta Phys. -Chim. Sin.* **36**, 1907004 (2020).

29. J. Hwang, M. Kim, D. Campbell, H. A. Alsalman, J. Y. Kwak, S. Shivaraman, A. R. Woll, A. K. Singh, R. G. Hennig, S. Gorantla, M. H. Rüemmeli, M. G. Spencer, van der Waals epitaxial growth of graphene on sapphire by chemical vapor deposition without a metal catalyst. *ACS Nano* **7**, 385–395 (2013).

30. M. A. Fanton, J. A. Robinson, C. Puls, Y. Liu, M. J. Hollander, B. E. Weiland, M. LaBella, K. Trumbull, R. Kasarda, C. Howsare, J. Stitt, D. W. Snyder, Characterization of graphene films and transistors grown on sapphire by metal-free chemical vapor deposition. *ACS Nano* **5**, 8062–8069 (2011).

31. Z. Chen, H. Chang, T. Cheng, T. Wei, R. Wang, S. Yang, Z. Dou, B. Liu, S. Zhang, Y. Xie, Z. Liu, Y. Zhang, J. Li, F. Ding, P. Gao, Z. Liu, Direct growth of nanopatterned graphene on sapphire and its application in light emitting diodes. *Adv. Funct. Mater.* **30**, 2001483 (2020).

32. H. J. Song, M. Son, C. Park, H. Lim, M. P. Levendorf, A. W. Tsen, J. Park, H. C. Choi, Large scale metal-free synthesis of graphene on sapphire and transfer-free device fabrication. *Nanoscale* **4**, 3050–3054 (2012).

33. K. Jia, H. Ci, J. Zhang, Z. Sun, Z. Ma, Y. Zhu, S. Liu, J. Liu, L. Sun, X. Liu, J. Sun, W. Yin, H. Peng, L. Lin, Z. Liu, Superclean growth of graphene using a cold-wall chemical vapor deposition approach. *Angew. Chem. Int. Ed.* **59**, 17214–17218 (2020).

34. X. G. Wang, A. Chaka, M. Scheffler, Effect of the environment on alpha-Al_2O_3 (0001) surface structures. *Phys. Rev. Lett.* **84**, 3650–3653 (2000).

35. Z. Dou, Z. Chen, N. Li, S. Yang, Z. Yu, Y. Sun, Y. Li, B. Liu, Q. Luo, T. Ma, L. Liao, Z. Liu, P. Gao, Atomic mechanism of strong interactions at the graphene/sapphire interface. *Nat. Commun.* **10**, 5013 (2019).

36. J. Sun, Y. Chen, M. K. Priydarshi, Z. Chen, A. Bachmatiuk, Z. Zou, Z. Chen, X. Song, Y. Gao, M. H. Ruemmeli, Y. Zhang, Z. Liu, Direct chemical vapor deposition-derived graphene glasses targeting wide ranged applications. *Nano Lett.* **15**, 5846–5854 (2015).

37. H. Huang, W. Chen, S. Chen, A. T. S. Wee, Bottom-up growth of epitaxial graphene on 6H-SiC (0001). *ACS Nano* **2**, 2513–2518 (2008).

38. K. V. Emtsev, A. Bostwick, K. Horn, J. Jobst, G. L. Kellogg, L. Ley, J. L. McChesney, T. Ohta, S. A. Reshanov, J. Röhrl, E. Rotenberg, A. K. Schmid, D. Waldmann, H. B. Weber, T. Seyller, Towards wafer-size graphene layers by atmospheric pressure graphitization of silicon carbide. *Nat. Mater.* **8**, 203–207 (2009).

39. J. H. Cox, L. Pidgeon, An investigation of the aluminum–oxygen–carbon system. *Can. J. Chem.* **41**, 671–683 (1963).

40. X.-D. Chen, Z. Chen, W.-S. Jiang, C. Zhang, J. Sun, H. Wang, W. Xin, L. Lin, M. K. Priydarshi, H. Yang, Z.-B. Liu, J.-G. Tian, Y. Zhang, Y. Zhang, Z. Liu, Fast growth and broad applications of 25-inch uniform graphene glass. *Adv. Mater.* **29**, 1603428 (2017).

41. J. W. Suk, A. Kitt, C. W. Magnuson, Y. Hao, S. Ahmed, J. An, A. K. Swan, B. B. Goldberg, R. S. Ruoff, Transfer of CVD-grown monolayer graphene onto arbitrary substrates. *ACS Nano* **5**, 6916–6924 (2011).

42. P. Bøggild, D. M. Mackenzie, P. R. Whelan, D. H. Petersen, J. D. Buron, A. Zurutuza, J. Gallop, L. Hao, P. U. Jepsen, Mapping the electrical properties of large-area graphene. *2D Mater.* **4**, 042003 (2017).

43. C. Liu, X. Xu, L. Qiu, M. Wu, R. Qiao, L. Wang, J. Wang, J. Niu, J. Liang, X. Zhou, Z. Zhang, M. Peng, P. Gao, W. Wang, X. Bai, D. Ma, Y. Jiang, X. Wu, D. Yu, E. Wang, J. Xiong, F. Ding, K. Liu, Kinetic modulation of graphene growth by fluorine through spatially confined decomposition of metal fluorides. *Nat. Chem.* **11**, 730–736 (2019).

44. G. Kresse, J. Hafner, Ab initio molecular dynamics for liquid metals. *Phys. Rev. B* **47**, 558–561 (1993).

45. P. E. Blöchl, Projector augmented-wave method. *Phys. Rev. B* **50**, 17953–17979 (1994).

46. J. P. Perdew, K. Burke, M. Ernzerhof, Generalized gradient approximation made simple. *Phys. Rev. Lett.* **77**, 3865–3868 (1996).

47. H. J. Monkhorst, J. D. Pack, Special points for Brillouin-zone integrations. *Phys. Rev. B* **13**, 5188–5192 (1976).

48. J. Klimeš, D. R. Bowler, A. Michaelides, Van der Waals density functionals applied to solids. *Phys. Rev. B* **83**, 195131 (2011).

49. P. T. M. M. van Attekum, G. K. Wertheim, Excitonic effects in core-hole screening. *Phys. Rev. Lett.* **43**, 1896–1898 (1979).

50. S. Doniach, M. Sunjic, Many-electron singularity in x-ray photoemission and x-ray line spectra from metals. *J. Phys. C Solid State Phys.* **3**, 285–291 (1970).

51. S. Tang, H. Wang, H. S. Wang, Q. Sun, X. Zhang, C. Cong, H. Xie, X. Liu, X. Zhou, F. Huang, X. Chen, T. Yu, F. Ding, X. Xie, M. Jiang, Silane-catalysed fast growth of large single-crystalline graphene on hexagonal boron nitride. *Nat. Commun.* **6**, 6499 (2015).

52. W. S. Leong, H. Wang, J. Yeo, F. J. Martin-Martinez, A. Zubair, P.-C. Shen, Y. Mao, T. Palacios, M. J. Buehler, J.-Y. Hong, J. Kong, Paraffin-enabled graphene transfer. *Nat. Commun.* **10**, 867 (2019).

53. B. Deng, Z. Pang, S. Chen, X. Li, C. Meng, J. Li, M. Liu, J. Wu, Y. Qi, W. Dang, H. Yang, Y. Zhang, J. Zhang, N. Kang, H. Xu, Q. Fu, X. Qiu, P. Gao, Y. Wei, Z. Liu, H. Peng, Wrinkle-free single-crystal graphene wafer grown on strain-engineered substrates. *ACS Nano* **11**, 12337–12345 (2017).

54. J. Robinson, X. Weng, K. Trumbull, R. Cavalero, M. Wetherington, E. Frantz, M. LaBella, Z. Hughes, M. Fanton, D. Snyder, Nucleation of epitaxial graphene on SiC (0001). *ACS Nano* **4**, 153–158 (2010).

55. J. Kim, H. Park, J. B. Hannon, S. W. Bedell, K. Fogel, D. K. Sadana, C. Dimitrakopoulos, Layer-resolved graphene transfer via engineered strain layers. *Science* **342**, 833–836 (2013).